This is a repository copy of *Observations of the variation in aerosol and cloud microphysics along the 20°s transect on 13 november 2008 during VOCALS-REx*.

White Rose Research Online URL for this paper:
http://eprints.whiterose.ac.uk/80172/

Version: Published Version

Article:

Observations of the Variation in Aerosol and Cloud Microphysics along the 20°S Transect on 13 November 2008 during VOCALS-REx

ZHIQIANG CUI

Institute for Climate and Atmospheric Science, School of Earth and Environment, University of Leeds, Leeds, United Kingdom

ALAN GADIAN AND ALAN BLYTH

National Centre for Atmospheric Science, University of Leeds, Leeds, United Kingdom

JONATHAN CROSIER

National Centre for Atmospheric Science, University of Leeds, Leeds, and Centre for Atmospheric Science, School of Earth, Atmospheric and Environmental Sciences, University of Manchester, Manchester, United Kingdom

IAN CRAWFORD

Centre for Atmospheric Science, School of Earth, Atmospheric and Environmental Sciences, University of Manchester, Manchester, United Kingdom

ABSTRACT

Observations are presented of the structure of the marine boundary layer (MBL) in the southeastern Pacific made with the U.K. BAe 146 aircraft on 13 November 2008 as it flew at a variety of altitudes along 20°S between the coast of Chile and a buoy 950 km offshore during the Variability of American Monsoon Systems (VAMOS) Ocean–Cloud–Atmosphere–Land Study (VOCALS) Regional Experiment (REx). The purpose of the study is to determine the variations along the 20°S transect in the clouds and boundary layer on this particular day as compared to the typical structure determined from the composite studies. The aircraft flew in three regions on this day: relatively continuous thick stratocumulus clouds, open cells, and closed cells. Results show three particular features. First, the results of the cloud microphysics are consistent with the typical behavior showing a decrease in aerosol particles by a factor of 3–4, and a decrease in cloud droplet number concentration westward from the coast from about 200 to $100\,\mathrm{cm}^{-3}$ or less with a corresponding increase in the concentration of drizzle drops with a maximum in open cells. Sulfate was dominant in the aerosol mass. Second, there was evidence of decoupling of the marine boundary layer that coincided with a change in the cloud type from stratiform to convective. The case differs from the average found in VOCALS in that the decoupling is not consistent with the deepening–warming idea. Precipitation is thought to possibly be the cause instead, suggesting that aerosol might play a controlling role in the cloud–boundary layer structure. Finally, cold pools were observed in the MBL from the dropsonde data.

Corresponding author address: Zhiqiang Cui, Institute for Climate and Atmospheric Science, School of Earth and Environment, University of Leeds, Woodhouse Lane, Leeds LS2 9JT, United Kingdom.
E-mail: z.cui@leeds.ac.uk

1. Introduction

In the southeastern Pacific off the South American coast, the marine boundary layer (MBL) is commonly capped by an extensive deck of stratocumulus clouds

with a strong inversion at cloud top (Painemal et al. 2010). The depth of the MBL, entrainment at the cloud top, and decoupling, among other factors, can affect the MBL structure and clouds (Wood and Bretherton 2004). Observations made by Rahn and Garreaud (2010a) during the Variability of American Monsoon Systems (VAMOS) Ocean–Cloud–Atmosphere–Land Study (VOCALS) showed that southeasterly trade winds normally less than $10 \, m \, s^{-1}$ prevailed within the MBL during the VOCALS period (October–November 2008), although the wind speed decreased toward the coast. They also found that the strongest inversion was observed between 74° and 76°W. Bretherton et al. (2010) found that the boundary layer was typically 1 km deep in the coastal zone, fairly well mixed, and topped by thin stratocumulus that contained negligible drizzle. Far offshore (1000 km or more), the boundary layer depth was typically deeper (about 1600 m) and thermodynamically more variable.

The subcloud layer can become decoupled from the layer near the surface by several processes. The decoupling may be driven by more radiative heating on the cloud layer than the layer below as a result of diurnal variation (Nicholls 1984), by cooling the subcloud layer through drizzle evaporation (Brost et al. 1982) or by negative buoyancy fluxes below the cloud layer during cloud thickening when the sea surface underneath the MBL is warmer (Bretherton and Wyant 1997). Jones et al. (2011) analyzed data up to 1600 km offshore from VOCALS and found that the main explanation for decoupling events was the deepening–warming theory (Bretherton and Wyant 1997).

One consequence of the decoupling is the formation of shallow cumulus cells in the subcloud layer because moisture and potential energy can accumulate in the lower layer. For example, Jensen et al. (2000) studied the MBL that contained both cumulus clouds and an upper-level stratus deck organized in a closed cell circulation. They observed new convective elements in a band shape using video recordings and photographs and termed it as the boundary layer squall line. Comstock et al. (2005) found that individual cells have lifetimes of up to 2 h.

The aerosol size, concentration, and chemical composition varied significantly with longitude within the MBL in VOCALS (e.g., Bretherton et al. 2010). There was generally a more variable and polluted coastal environment and a less variable, more pristine maritime environment (Bennartz 2007; Tomlinson et al. 2007; Bretherton et al. 2010; Allen et al. 2011). Bretherton et al. (2010) found that in the coastal zone, boundary layer air along 20°S usually had a back trajectory that intersected Chilean coastal pollution sources; in the transition zone, land contact was made only in some trajectories; while those in the remote zone did not pass over land. For the free-troposphere air masses, they found a variable and complex vertical interleaving of air masses from diverse sources. Allen et al. (2011) analyzed the back trajectories of air masses of the MBL at 20°S in the VOCALS region. They found three distinctive longitudinal zones: a coastal zone (70°–75°W), a transition zone (75°–80°W), and a remote zone (80°–85°W). The sources of aerosol over Chile are usually biomass burning, sea surface, an urban biofuels mix, and a somewhat ambiguous mix of smelter emissions and mineral dust (Chand et al. 2010). The dominant identified aerosol smaller than $1 \, \mu m$ is sulfate, but much of the unidentified mass is likely organic (Chand et al. 2010). As expected, the variation in cloud drop number concentration observed was closely associated with the strong gradient in aerosol (Allen et al. 2011). Bretherton et al. (2010) suggested that there were local and more variable coastally dominated pollutant sources for free-troposphere air masses to the east of 74°W and more diverse pollutants from a variety of long-range sources to the west of 74°W.

Kazil et al. (2011) simulated the chemical and aerosol processes in the transition from closed to open cells in VOCALS with the Advanced Research Weather Research and Forecasting Model coupled with chemistry (ARW-Chem). They found that an ultraclean layer developed below the inversion base by cloud scavenging during the transition. Convective updrafts in the open cell wall lifted dimethyl sulfide (DMS) from the ocean surface into the ultraclean layer, where new aerosol particles formed efficiently through oxidation and chemical processes.

Bennetts et al. (1986) summarized the physical processes that are important to the development of stratocumulus (Sc): surface fluxes of heat and moisture, synoptic anticyclonic subsidence, cooling and heating due to longwave radiation, turbulent entrainment at cloud top, turbulent mixing in cloud, and microphysical processes. The formation and evolution of stratocumulus clouds involve complex interactions of these processes on various scales. A solid stratus layer may become broken by cloud-top entrainment instability (e.g., Klein et al. 1995). Sometimes, open and closed cells are seen by satellite images (e.g., Bretherton et al. 2004). The closed cells are a regular array of cloud with a connecting lattice of clear air, while the open cells are a regular array of clear patches with a connecting lattice of cloud. Both features may organize as pockets of open cells (POCs); that is, the open cells are entirely surrounded by closed cells (Bretherton et al. 2004; Stevens et al. 2005). The transition from closed to open cells has attracted significant research interest especially in the last decade because of the interaction between aerosol, clouds, precipitation, and the impact on radiation and climate (Stevens et al. 2005).

Drizzle formation in stratocumulus clouds depends on both micro- and macroproperties of clouds. For example, Pawlowska and Brenguier (2003) found that the drizzle rate could be parameterized as approximately H^3/CDNC, where H is the cloud depth and CDNC is the cloud drop number concentration. Drizzle can develop in Sc clouds when the concentration of cloud condensation nuclei (CCN) is low or the cloud is deep, so that cloud drops are large and the collision–coalescence process is more efficient. Yum and Hudson (2004) observed anticorrelation between CCN number and drizzle in marine stratocumulus. Drizzle most frequently occurs in the early morning as a result of nighttime thickening of the cloud layer in the MBL (Comstock et al. 2005).

Recent studies have found that drizzle drops are necessary but not sufficient for the formation and maintenance of POCs (Comstock et al. 2005; Stevens et al. 2005; Sharon et al. 2006; Wood et al. 2011a). Heavy drizzle from cells in the transition zone between closed and open cells have been observed (Savic-Jovcic and Stevens 2008; Wood et al. 2011a). These transition cells usually have cold and moist pools below the precipitating clouds (Wood et al. 2011a).

Drizzle can reduce the aerosol concentration by impaction scavenging, which enhances drizzle until an ultraclean state is reached (Sharon et al. 2006). The ultraclean environment promotes new aerosol particle formation. DMS from the ocean surface is transported in the open cell wall updraft into the ultraclean layer below the cloud base and becomes H_2SO_4 through sulfate chemical processes. Kazil et al. (2011) found that the observed DMS flux from the ocean in the VOCALS region can support a nucleation source of aerosol in open cells that exceeds sea salt emissions in terms of the number of particles produced. However, the newly nucleated, nanometer-sized aerosol particles would need time to grow to sizes large enough to act as CCN.

Aircraft observations by Wood et al. (2011a) revealed the fine details of the transition from closed to open mesoscale cellular convection. The transition zone between the POC and the closed cells often consisted of thick "boundary cell" clouds with heavy drizzle, a divergent quasi-permanent cold/moist pool below cloud, a convergent inflow region at midlevels in the MBL, and a divergent outflow near the top of the MBL. They concluded that drizzle alone is not sufficient for a POC to form.

In this paper, we present a detailed analysis of the aerosol particles and the microphysical properties of the clouds observed along 20°S on 13 November 2008 with the BAe 146 research aircraft. Three different regions were sampled: stratocumulus, open cells, and closed cells. In addition, the early stage of development of a POC was encountered. The study complements previous studies of the average properties of the stratocumulus cloud-topped boundary layer system in the VOCALS region (Bretherton et al. 2010; Allen et al. 2011) and shows the details of the microphysical behavior along the 20°S transect. Section 2 describes the project and instruments used in the analysis of the case study. Section 3 presents the variations in aerosol and cloud microphysics, particularly drizzle. Finally, the discussion and conclusions are given in sections 4 and 5, respectively.

2. Observations

On 13 November 2008, the U.K. Facility for Airborne Atmospheric Measurements (FAAM) BAe 146 research aircraft flew between 72° and 81°W along 20°S latitude off the western coast of South America and made measurements of cloud microphysics, aerosol, chemistry, radiation, dynamics, and thermodynamics in the MBL. The BAe 146 flew with a mean speed of $100\,m\,s^{-1}$, typically for about 5 h, covering a range of about 900 km. The instruments on board the aircraft have been described in several VOCALS papers (e.g., Wood et al. 2011a,b; Allen et al. 2011). We briefly describe the relevant instruments used in this study.

The Nevzorov probe is a constant temperature, hot-wire probe that measures the liquid water content (LWC) and total water content. The measurement accuracy of the Nevzorov probe is given as ±10%–15% (Korolev et al. 1998). The Johnson–Williams (JW) probe measures LWC in clouds using a heated wire resistance bridge at a frequency of 4 Hz (Strapp and Schemenauer 1982). It is found that the JW probe underestimates the LWC as a result of an incomplete response to larger cloud droplets (Feind et al. 2000).

The Stratton Park Engineering Company (SPEC) two-dimensional stereo (2D-S) 128 shadow imaging probe uses a 128-photodiode linear array to detect the shadow of cloud particles passing through its sample volume, illuminated by the laser (Lawson et al. 2006). It produces two-dimensional images of particles in the cloud and counts and sizes particles from $10\,\mu m$ to 1.3 mm, with a response time of 41 ns. Its greatly improved determination of sample volume and sizing of small particles less than $100\,\mu m$ in diameter allows good measurements to be made of the development of drizzle (Crosier et al. 2011; Crawford et al. 2012; Cui et al. 2012; Crosier et al. 2014).

The Droplet Measurement Technologies (DMT) cloud droplet probe (CDP) measures the light scattered from a single droplet passing through an open-path laser beam. The CDP uses a diode laser, with a single-mode elliptical Gaussian beam roughly 2 mm × 0.2 mm, to count and size individual water droplets in the range 3–$50\,\mu m$ (Lance et al. 2010). There are 30 size bins with the bin width either of 1 or $2\,\mu m$.
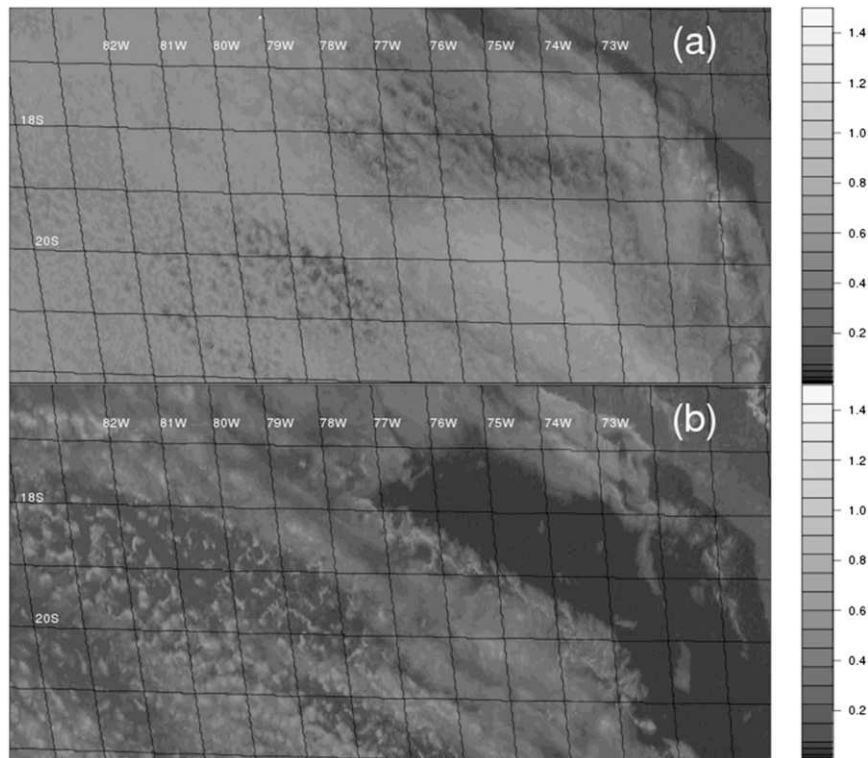
FIG. 1. *GOES-10* visible image at (a) 1215 and (b) 1945 UTC 13 Nov 2008.

The aerosol mass spectrometer (AMS) uses mass spectrometry to determine the chemical functionality of ionized fragments and retrieves the mass loading of the nonrefractory, non–sea salt chemical component of submicron aerosol, with a 30-s integration time in the case of the BAe-146 and a sampling size range of 0.04–0.7 μm (Jayne et al. 2000; Drewnick et al. 2005; Allen et al. 2011).

The aerosol size distribution is measured with the passive cavity aerosol spectrometer probe (PCASP), which has a nominal range from 0.1 to 3 μm. The PCASP is an optical particle counter. The size of each aerosol particle is calculated by measuring the forward-scattered light intensity as the particle passes through a focused laser beam (Allen et al. 2011; Blyth et al. 2013).

The Vaisala dropsonde RD93 measures the profiles of pressure, temperature, relative humidity, wind direction, and wind speed from the point of launch to the ground. The National Center for Atmospheric Research developed this global positioning system dropsonde system in cooperation with the German Aerospace Center and the National Oceanic and Atmospheric Administration. The resolution and uncertainty during the sounding of the pressure, temperature, relative humidity, and wind speed probes on the dropsonde are 0.1 and 1.5 hPa, 0.1° and 0.5°C, 1% and 5%, and 0.1 and 0.5 m s^{-1}, respectively.

3. Synoptic conditions and flight pattern

The synoptic conditions on 13 November 2008 were dominated by the high pressure system that was positioned off South America over the southeastern Pacific. They were similar to the climatological conditions in this region (Zuidema et al. 2009; Rahn and Garreaud 2010b). Toniazzo et al. (2011) examined the synoptic meteorology in the southeastern Pacific during VOCALS in October and November 2008. They found that from the end of October to the middle of November, there was little synoptic activity from midlatitude depressions. However, there were clear diurnal variations in cloud cover, with nearly solid stratus during the night and that broke up into stratocumulus during the day.

The satellite image taken at 1215 UTC 13 November 2008 (Fig. 1a) shows that there were stratocumulus clouds off the western coast of Arica Bay during the time of the BAe 146 flight. The image shows that, along 20°S, the Sc clouds were broken near the coast and more uniform, but still with substantial variability from about 72° to about 77°W. Cellular clouds had already formed to the west of 77°W along 20°S. The satellite image at 1945 UTC (Fig. 1b) indicates that a POC had become well developed between 77° and 82°W. The aircraft flew through the POC in its early development stage.
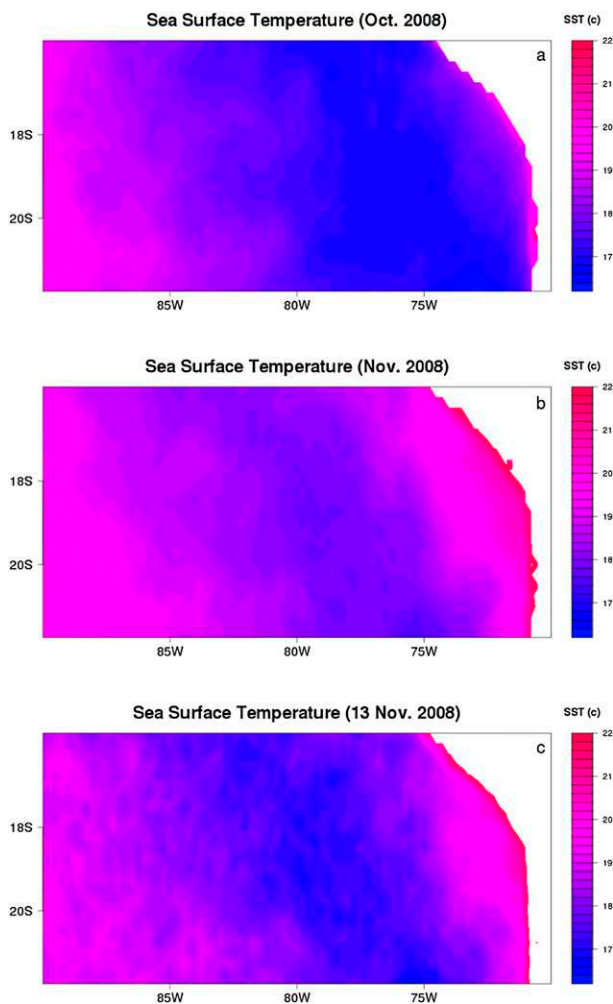
FIG. 2. TMI SST: (a) October mean, (b) November mean, and (c) 3-day mean ending on 13 Nov 2008.

FIG. 3. Flight pattern along 20°S latitude for 17 profile runs between P5 and P21, and 9 SLRs, R4.1–R.7.2 from point α (20°S, 72°W).

Figure 2 shows the sea surface temperature (SST) derived by the Tropical Rainfall Measuring Mission (TRMM) Microwave Imager (TMI). The variation of SST along 20°S is different between October and November. SSTs were lower to the east of 80°W than to the west in October, except for a very narrow zone of high SST near the coast. In contrast, SSTs along 20°S are lower between 80° and 75°W than to either east or farther west in November. The spatial variation in 3-day-mean SST ending on 13 November 2008 along 20°S (Fig. 2c) is similar to the monthly mean of November; that is, the lower SSTs were between about 80° and 75°W along 20°S.

Five aircraft mission strategies were adopted during VOCALS (Wood et al. 2011b). One of the strategies used on 13 November 2008 is the cross-section mission along 20°S latitude aiming to sample longitudinal gradients in the properties of the aerosol and the Sc clouds,
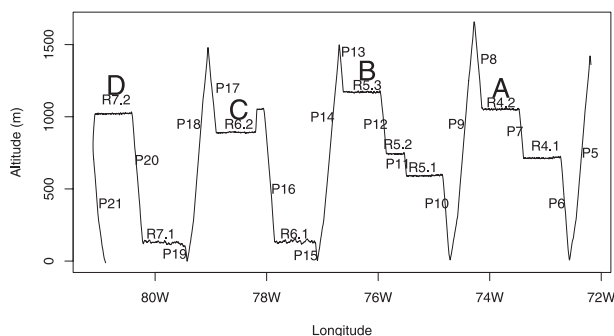
and the characteristics of the marine boundary layer. The BAe 146 flight plan is shown in Fig. 3. The aircraft took off from Arica, Chile (18°S, 70°W), and flew to point α (20°S, 72°W). There were four profile runs and three straight-and-level runs (SLRs) before the aircraft arrived at 20°S. The aircraft sampled westward along 20°S to 81.113°W, and 17 profiles runs and 9 SLRs were made. The SLRs consisted of four in-cloud runs (runs 4.2, 5.3, 6.2, and 7.2, referred to as runs A, B, C, and D, respectively) and five below-cloud runs (runs 4.1, 5.1, 5.2, 6.1, and 7.1). One (runs 4.1, 6.1, and 7.1) or two (runs 5.1 and 5.2) below-cloud runs were conducted to examine the aerosol properties below cloud bases before each in-cloud run was performed to measure the cloud properties. The profile runs (runs P5–P21) were carried out to record the vertical variations in aerosol, cloud, and meteorological parameters. Then, the aircraft ascended to about 7000 m MSL in profile 22 and a sonde was dropped at 5500 m during ascent. Nine more sondes were dropped roughly every 100 km along a straight-and-level run from 20°S, 80°W to 20°S, 72°W at 7000 m MSL. Two sondes fell into the region of the POC. Finally, a profile run (profile 23) was made before the aircraft landed. Figure 3 shows the longitude and altitude of the aircraft along 20°S between profiles 5 and 21.

The flight tracks were superimposed on satellite images for the SLRs (Fig. 4). The aircraft flew through the solid Sc deck in run B (Fig. 4a), open cells in run C (Fig. 4b), and closed cells in run D (Fig. 4c).

4. Results

Figure 5 shows a summary of the boundary layer and cloud properties observed during the 20°S transect from near the coast of Chile about 950 km westward. The properties were similar to the average conditions reported by Bretherton et al. (2010) and Allen et al. (2011) for the VOCALS project, except that the SSTs were higher in the eastern portion of the transect (Fig. 5a).
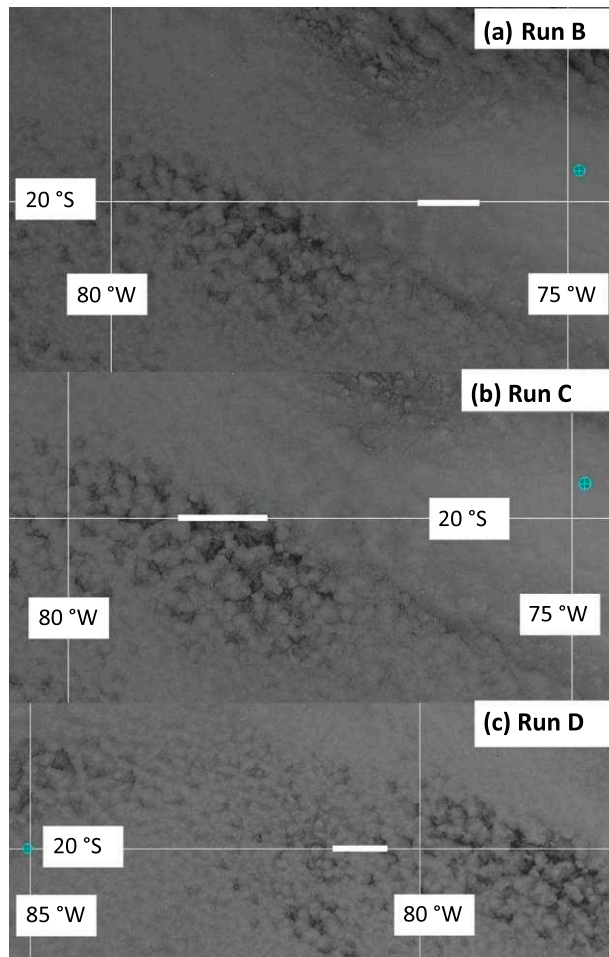
FIG. 4. Flight tracks for runs 5.3 (run B), 6.2 (run C), and 7.2 (run D) superimposed on *GOES-10* visible images. (a) Run 5.3 was between 1134:45 and 1144:46 UTC and the image was taken at 1145 UTC. (b) Run 6.2 was between 1206:49 and 1219:51 UTC and the image was taken at 1215 UTC. (c) Run 7.2 was between 1243:04 and 1253:07 UTC and the image was taken at 1245 UTC.

The aerosol concentration, and consequently the concentrations of cloud droplets, was much higher close to the coast than in the west. Figure 5 shows, however, that the decrease occurred over a distance of approximately 140 km from 74.7° to 76°W (considering the straight-and-level runs only). The concentration of cloud droplets decreased from about 300 to less than 60 cm^{-3}. The mean values of LWP with the *Geostationary Operational Environmental Satellite-10* (*GOES-10*) measurement in runs A–D are 113.63, 183.68, 172.15, and 192.98 g m^{-2}, respectively, and these values did not vary significantly in runs B–D. However, there are some high values of LWP between 75° and 76°W in the overcast region, which had a deep cloud layer but very light drizzle. Figure 5d also shows the now-familiar aerosol–precipitation relationship—the amount of precipitation

was greater in clouds with lower concentrations of cloud drops. However, there is a bit more of a jump in the amount of precipitation than might be expected from a simple aerosol–cloud–precipitation interaction argument. This is explored further below.

a. Variability in aerosol properties

Figure 5b shows the longitudinal variation of aerosol concentration measured with the PCASP. The concentration was a relatively constant value of between 400 and 500 cm^{-3} in the straight-and-level out-of-cloud runs at an altitude between 550 and 750 m MSL to the east of 74°W. The concentration began to decrease from 700 to 300 cm^{-3} between 74° and 76°W. The aircraft did not do a run at this altitude again in this flight. The concentration was less than 200 cm^{-3} to the west of 76°W at an altitude of about 100 m MSL. The vertical profiles add to this picture of the concentration of the aerosol particles.

The vertical variation of aerosol concentration for the 23 profile runs made on this flight is shown in Fig. 6. The concentrations in the MBL can be grouped in three zones. In the first zone close to the coast (east of 72°W), the mean concentrations in the MBL were about 1000 cm^{-3}. Profiles 1, 2, 3, and 23 were made in the zone close to the coast. In the transition zone between 72° and 76°W (profiles 5–13), the mean concentrations were about 500 cm^{-3}. Farther offshore to the west of 76°W, the mean concentrations were between 50 and 150 cm^{-3}. In run 7.1, drizzle was observed with the 2D-S at about 127 m MSL. The particularly low concentration of aerosol particles is presumably the result of scavenging by drizzle (Wood et al. 2012). The longitudinal variation in this case agrees with the statistical results from VOCALS (Allen et al. 2011; Bretherton et al. 2010).

Figure 7 shows the vertical variation of the chemical composition of aerosol measured with the AMS during the 23 profiles. We focus on the variations below 2000 m MSL. Figure 7a shows that sulfate aerosol dominated the aerosol mass, followed by ammonium and organics, with only a small contribution from nitrate and chloride (Fig. 7a). Sulfate and ammonium aerosol masses decreased as the aircraft flew offshore (Figs. 7b,d). There are various sources of sulfate aerosol near and off the coast. Sulfur dioxide emission from copper smelters is the main continental source of sulfate aerosol (Artaxo et al. 1999; Carn et al. 2007). The marine source of sulfate aerosol is likely from the oxidation products of DMS and methyl sulfonic acid (Ayers et al. 1991; Mari et al. 1998), as well as the direct oxidation of SO$_2$ in cloud droplets (Sievering et al. 1992; O'Dowd et al. 1997; Andreae et al. 1999). Allen et al. (2011) suggested that the sulfate and ammonium aerosol have a predominantly marine source in the remote MBL of the
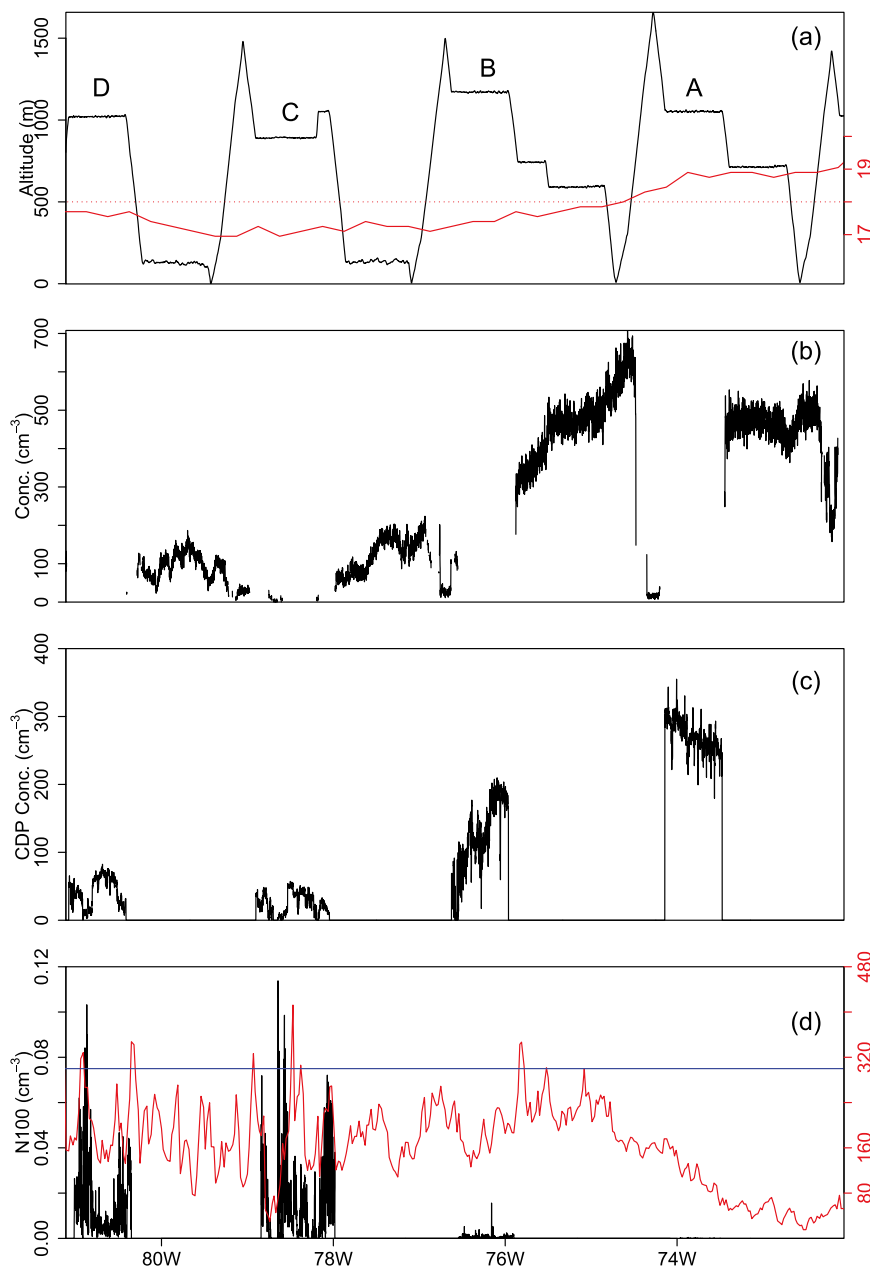
FIG. 5. Longitudinal variation of (a) aircraft height (black) and daily-mean SST (red; °C) along 20°S, (b) aerosol concentration measured with the PCASP in the size range between 0.15 and $3\,\mu m$, (c) drop concentration measured with the CDP, and (d) concentration of drops whose diameter is greater than $100\,\mu m$ measured with the 2D-S; the red line is the *GOES-10* LWP $(g\,m^{-2})$ and the blue line represents LWP $= 300\,g\,m^{-2}$.

VOCALS region and the concentration was low as a result. The organic aerosol (Fig. 7c) also decreased toward the west, most likely because the main sources of organics are fossil fuel and biomass burning. The reason for the offshore decrease in nitrate and chloride aerosol is less clear (Figs. 7e,f).

The average chemical composition obtained from the AMS is shown in Fig. 8 for each of the subcloud runs

4.1, 5.1, 6.1, and 7.1. As discussed above, the primary chemical composition in all four runs is sulfate, followed by organics and ammonium. Nitrate and chloride have the least mass, even in runs very close to the sea surface (runs 6.1 and 7.1). The dominance of the sulfate mass fraction over other aerosol components obtained with the AMS was shown by Allen et al. (2011) for four cases of longitudinal sampling with the BAe 146. The absolute
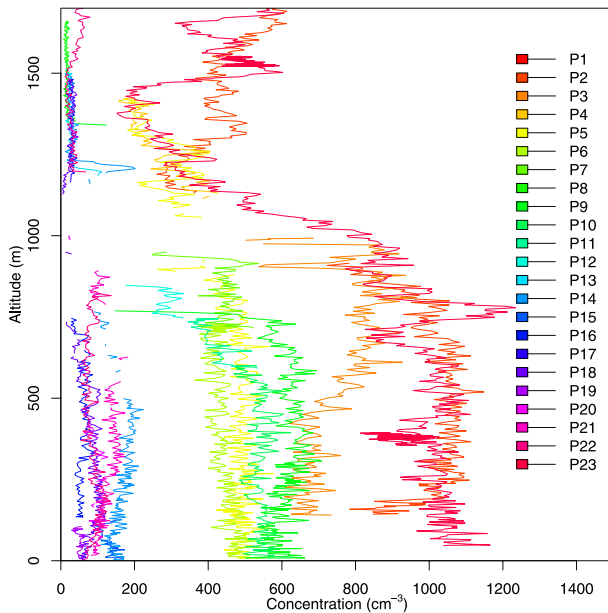
FIG. 6. Vertical variation of aerosol concentration measured with the PCASP in the size range between 0.15 and 3 μm during 23 profiles. See Fig. 3 and text for locations of the profiles.

values of aerosol mass in the four runs here show clear longitudinal variations as expected. The aerosol mass has a similar longitudinal pattern to the aerosol number concentration (Fig. 5b).

The concentration of the coarse-mode aerosol does not change significantly along 20°S (figure not shown). The wind speeds at the lowest points of profile runs P9, P14, P18, and P21 were 3.6, 3.29, 6.27, and 3.85 m s^{-1}, respectively. The values of the wind speeds were similar except for P18, which was taken in the POC region where local gusts from cold pools might have played a role. Since sea salt aerosol production is mainly dependent on wind speed near the sea surface, it is suggested that sea salt could be the main source of coarse aerosol. This is consistent with the results of Kazil et al. (2011), who found that mechanical production of sea salt aerosol provides a steady source of larger particles that are effective CCN at a rate exceeding a threshold for maintenance of open cell circulation.

The ratio of organics to sulfate is a measure of the degree of lack of anthropogenic influence of the MBL. The range of the ratio in the four runs is between 0.08 and 0.36, indicating a very clean MBL (Shank et al. 2012; O'Dowd and de Leeuw 2007). The range in change for chloride in the four runs is about threefold, lower than in ammonium (fivefold), nitrate (fivefold), and organics (21-fold).

b. Variability in cloud properties

Figure 9 shows the longitudinal variation of cloud microphysical properties of the in-cloud runs A–D.

In run A, the aircraft penetrated the solid cloud layer from 73.476° to 74.141°W at an altitude of about 1 km MSL. The value of LWC increased slightly toward the west during the run (Fig. 9a). The mean and maximum values of LWC were about 0.152 and 0.236 g m^{-3}, respectively. The mean value of CDNC across the penetration was about 270 cm^{-3}, but as Fig. 9b shows, the value increased from about 200 to about 300 cm^{-3} from the beginning of the run to the end. The increased CDNC toward the west was related to the increased aerosol concentration in this run.

The concentration of drops with diameters greater than 50 μm was low (Fig. 9c); and the mean value was about 0.0018 cm^{-3}. The concentration of drizzle drops ($d > 100 \mu$m) was negligible. There are only small longitudinal variations until the end of the run, when the mean size increases (Fig. 9e).

In run B, the cloud penetration was carried out between 75.963° and 76.623°W at an altitude of about 1.2 km MSL (Fig. 5a). The aircraft flew close to cloud top to the west of 76.4°W. The mean value of LWC was 0.378 g m^{-3}, more than double the value measured in run A (Fig. 9a). The values of LWC in run B were higher than in run A because this run was conducted at a higher level above the cloud base (about 310 m) than in run A (about 100 m). The mean value of CDNC was about 124 cm^{-3}, much lower than that in run A. The concentration decreased westward from about 180 cm^{-3} near 76°W to 50 cm^{-3} near 76.6°W (Fig. 5d). There are significant fluctuations in both CDNC and LWC. The fluctuations are much greater than those experienced in run A, presumably because the aircraft was closer to cloud top (e.g., Gerber et al. 2005). The value of LWC decreases to almost zero during the two events.

The mean concentration of drops larger than 50 μm (N50) was 0.02 cm^{-3}, much higher than the observed value in run A. Also, the number concentration increased from about 0.02 to about 0.08 cm^{-3} from east to west. In fact, perhaps not surprisingly, there was an anticorrelation between N50 and CDNC during this single run. This is further illustrated by the increase in mean size of the cloud drop size distribution shown in Fig. 9e. The mean concentration of drizzle drops was only about 0.5 L^{-1}. However, the value was greater than the value of 0.01 L^{-1} measured during run A.

The aircraft flew in run C between 78.046° and 78.900°W at an altitude of about 1050 m in the beginning and descended to about 890 m because the cloud top varied. The early stages of development of the POC were observed near 78.7°W. It is clear from Figs. 4 and 9 that the clouds were less homogeneous and more cumuliform in structure. The mean value of CDNC was only about 25 cm^{-3} in this run, more than 10 times lower
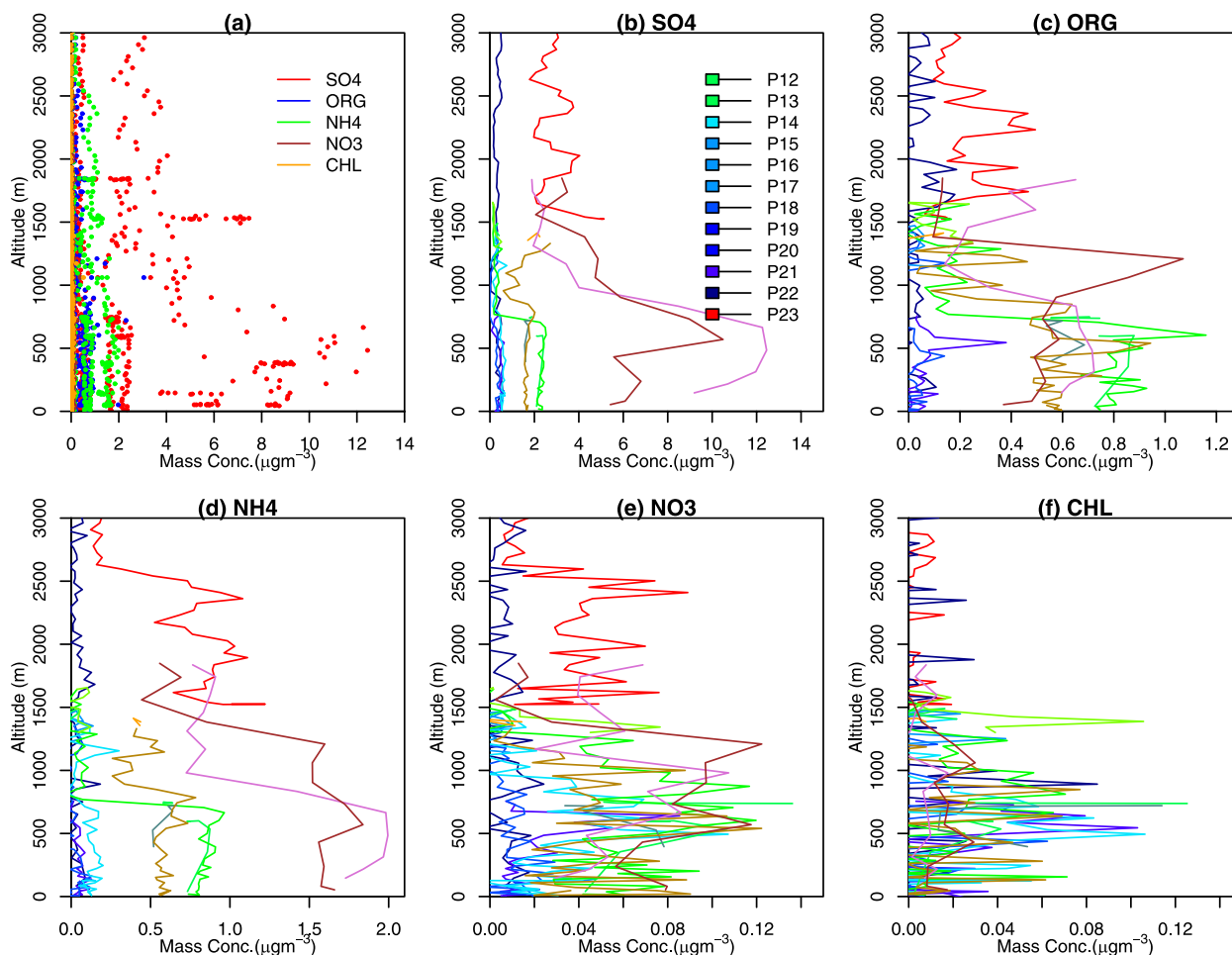
FIG. 7. Vertical variation of aerosol composition made with the AMS: (a) all species, (b) sulfate, (c) organics, (d) ammonium, (e) nitrate, and (f) chloride during 23 profiles.

than that measured in run A and about 5 times lower than in run B. The maximum concentration was less than $60 \, \mathrm{cm}^{-3}$, but the maximum LWC was about $0.5 \, \mathrm{g \, m}^{-3}$, which was less than the value measured in run B. The cloud drop size distribution (Fig. 9e) shows that there was substantial variability in the mean and maximum size of cloud drops. The concentration for drops larger than $50 \, \mu\mathrm{m}$ was much higher than in the previous run. The mean value was about $0.35 \, \mathrm{cm}^{-3}$. However, the maximum value was about $2 \, \mathrm{cm}^{-3}$. The concentration of drizzle drops was also significantly greater than in the cloud farther east. Values greater than $600 \, \mathrm{L}^{-1}$ were not uncommon (Fig. 9d).

Run D was made between 80.413° and 81.078°W at an altitude of about 1020 m MSL to the west of the developing POC in closed cells (Figs. 4c and 5a). The difference between the clouds in this region and to the east of the POC is the change in cloud types. Cellular clouds were observed in this region, while the

clouds were stratiform to the east. The mean value of CDNC was $42 \, \mathrm{cm}^{-3}$, less than that measured in runs A and B and approximately the same as that in run C. In fact the microphysical properties of the clouds were
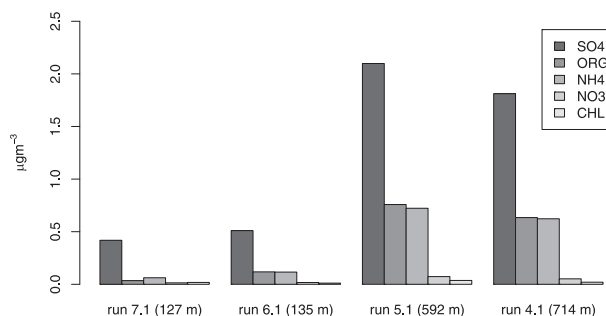

FIG. 8. Average aerosol composition from the AMS during four below-cloud-base runs. The heights of runs 4.1, 5.1, 6.1, and 7.1 are 714, 592, 135, and 127 m MSL, respectively. For longitude and altitude of the runs, see Fig. 2.

FIG. 9. Longitudinal variation of the four in-cloud runs: (a) LWC made with the Nevzorov probe, (b) drop number concentration made with the CDP, (c) number concentration of drops larger than 50 μm made with the 2D-S, (d) number concentration of drops larger than 100 μm made with the 2D-S, and (e) drop number size distribution made with the CDP. In (e), the y axis is the size up to 50 μm, and the color key to the right is the concentration of drops in each size bin.

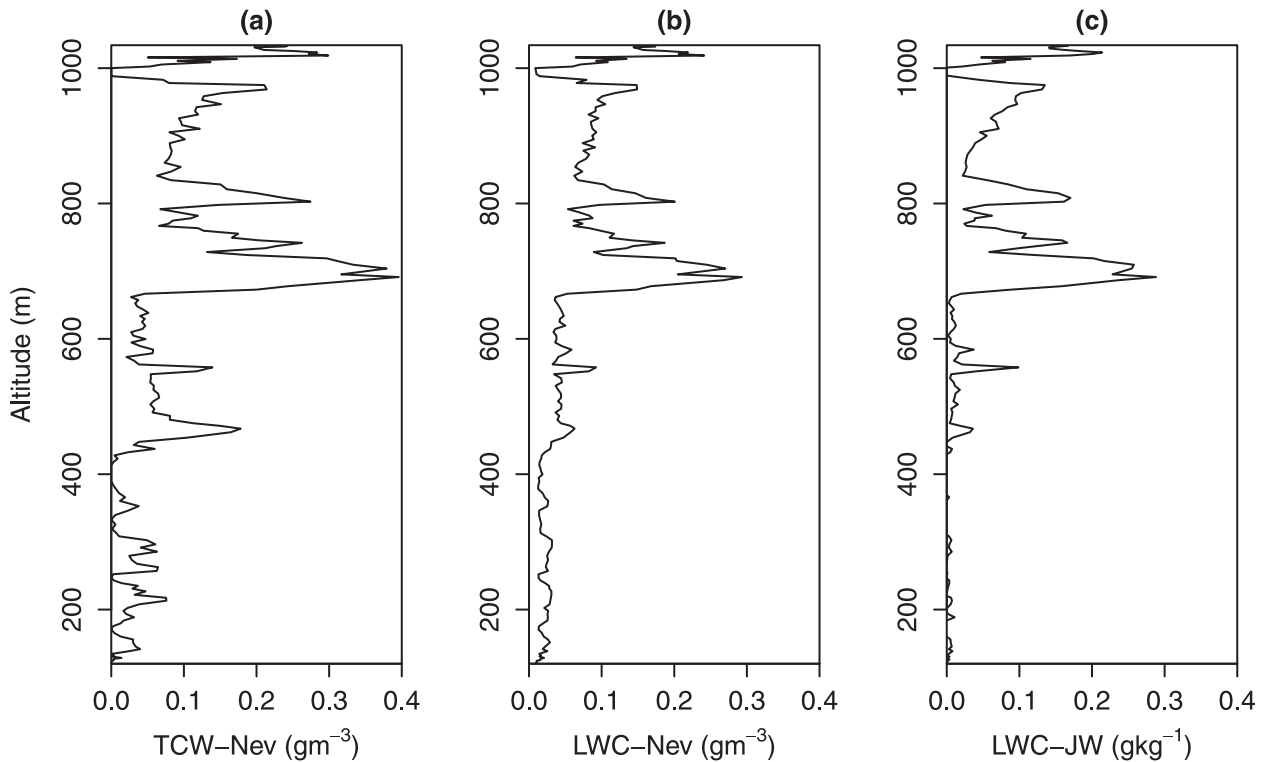FIG. 10. Vertical variation of (a) total condensed water, (b) LWC measured with the Nevzorov probe, and (c) LWC made with the JW probe during P20 (see Fig. 3).

similar to those measured in the open cells during run C (Fig. 9).

It is clear from Fig. 9d that there was a higher concentration of drizzle in clouds to the west of 77°W, where the concentration of aerosol particles was about 3–4 times lower than to the east of 77°W. Another factor for the enhanced drizzle was the transition of cloud types from stratiform to cumuliform (Comstock et al. 2007).

Runs 4.1, 5.1, and 5.2 were made just below cloud base at altitudes of about 714, 592, and 742 m, respectively, in the eastern part of the domain. No drizzle drops were detected in run 4.1, but a low concentration was measured in runs 5.1 and 5.2, as expected from what was observed in the cloud penetrations. Drizzle drops were recorded in some profiles, particularly profile 20. Figure 10 shows that drops were measured below cloud base (660 m) with the Nevzorov total condensed water and LWC probes as well as the JW LWC probe.

c. Decoupling, above cloud condition, and cold pools

The vertical variations of the liquid potential temperature and the liquid water mixing ratio for three profile runs—P9, P14, and P18—are shown in Fig. 11.

The liquid potential temperature θ_l is conserved in moist adiabatic processes (Betts 1973). It can be approximated as

$$\theta_l \approx \theta - \frac{L}{c_p} q_l, \tag{1}$$

where θ is the potential temperature, L is the latent heat of vaporization for water, c_p is the specific heat of dry air at constant pressure, and q_l is the liquid water mixing ratio.

The MBL was deeper in P9 (~1340 m) than in P14 (~1180 m) and P18 (~1130 m). The deeper cloud layer observed in P9 is likely associated with the higher SSTs close to the coast (Fig. 2), as suggested by the deepening–warming theory (Bretherton and Wyant 1997). Usually a deeper MBL is associated with decoupling in the deepening–warming theory and that was true in the typical cases described by Jones et al. (2011) during VOCALS. However, the deeper MBL in the east was well mixed (Fig. 11a) compared with the vertical profiles of θ_l in P14 and P18 in the west (Figs. 11b,c). The relative humidity profiles measured with the dropsondes show the signals of decoupling to the west of 78°W (bluish lines in Fig. 14a for DS1, DS2, and DS3).

The diurnal variation in radiation (Nicholls 1984) is an unlikely explanation for the decoupling in this case, since the aircraft measurements were taken in the early morning. In fact, Jones et al. (2011) concluded that the deepening–warming mechanism could broadly explain the decoupling events during VOCALS. The MBL was
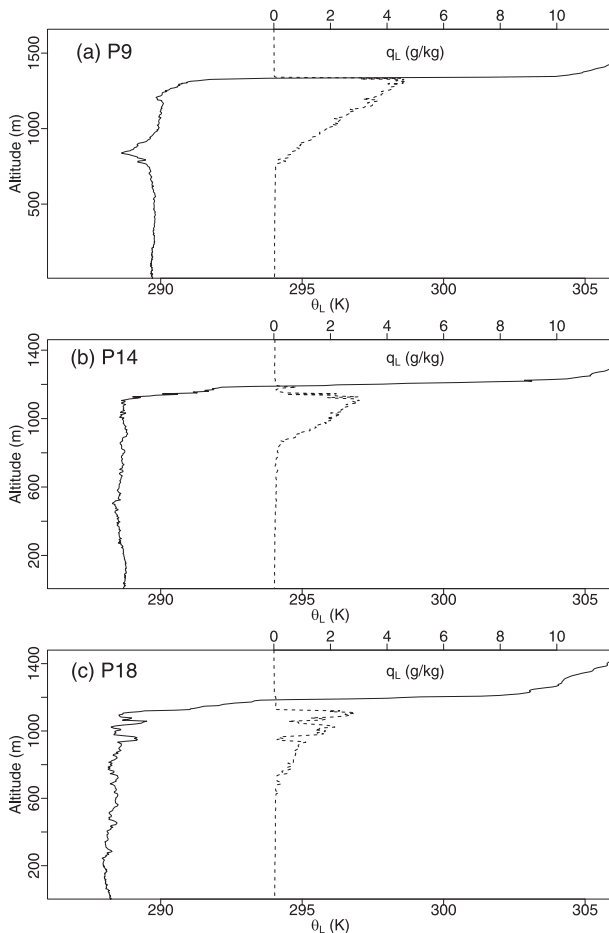
FIG. 11. Profiles of the liquid potential temperature (solid line) and the liquid water mixing ratio (dotted line) during profiles runs (a) P9, (b) P14, and (c) P18. The liquid water mixing ratio is multiplied by 10 for clear viewing. Please note that the *y* axis has different scales. See Fig. 3 for locations.

FIG. 12. Vertical variation in (a) relative humidity and (b) temperature above cloud top during three profile runs.

deep and the cloud layer was thicker near the coast along 20°S, and the MBL was well mixed in profile run P9. The reason for the deeper MBL close to the coast is the reversed SST pattern in November compared with the SST in October. The decoupling did not occur in the deeper MBL close to the coast, where SSTs were higher. This difference and the fact that the decoupling occurred when there was drizzle suggests that the decoupling was related to drizzle rather than the deepening–warming mechanism.

It has been known that the interaction between the MBL and the large-scale meteorology, such as free-tropospheric moisture and stability, can affect the clouds at the MBL top (Wood 2012). Figure 12 shows the vertical profiles of relative humidity and temperature above cloud top measured in profiles runs P8, P13, and P17. Both the relative humidity and the temperature changed very little from run to run. This suggests that the
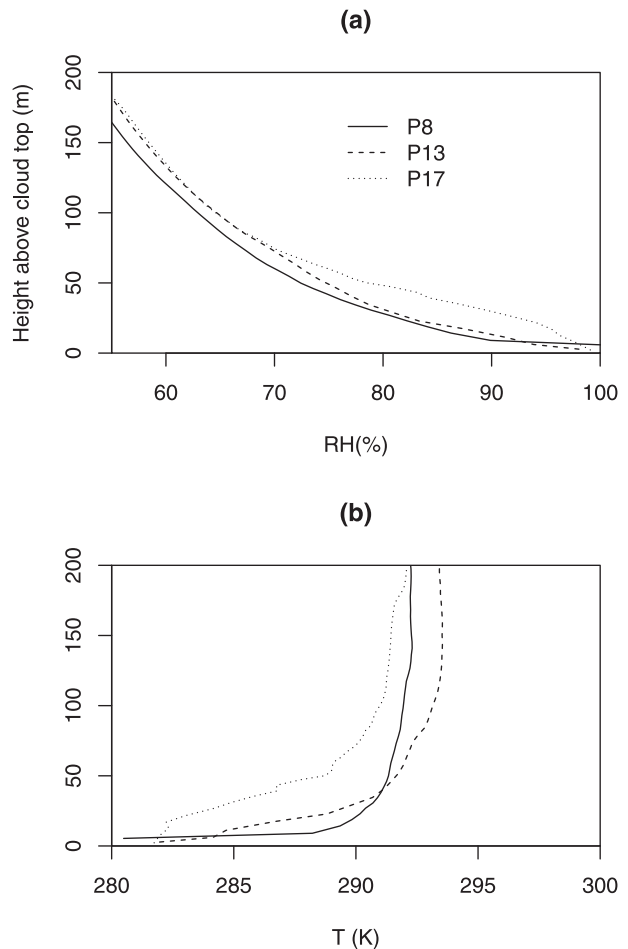
environment above the clouds was not the cause of the decoupling of the boundary layer or the deepening of the clouds toward the east.

Ten sondes were dropped at about a 1° interval on the return journey (Fig. 13). Table 1 presents the latitudes and longitudes of the sondes when they reached the lowest level.

The profiles of relative humidity and horizontal wind speed measured with the sondes are shown in Fig. 14. Figure 14a shows the variation from east to west and the relatively sharp transition from well mixed to variable profiles in the boundary layer, which is consistent with Fig. 11 and the decoupling. There was a sharp increase in relative humidity in the lowest 100 m in dropsonde 2, clear evidence of moistening due to evaporation.

The east–west horizontal wind speed in Fig. 14b shows that dropsonde 3 evidently fell through a cold pool similar to those produced by convective clouds. The westerly wind speed increased significantly to about 5 m s^{-1} at an
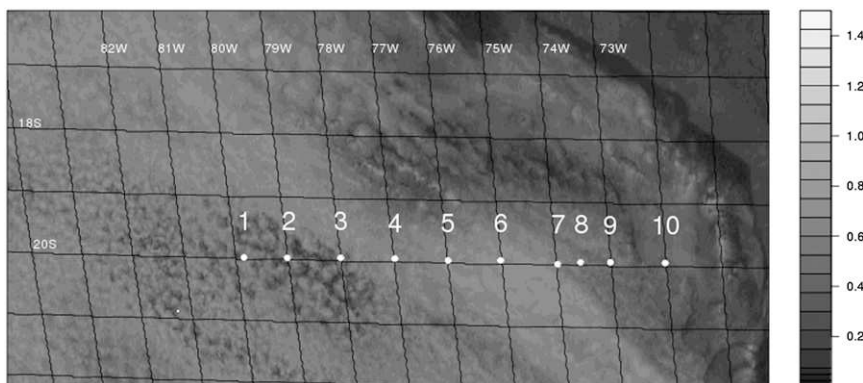
FIG. 13. Visible image from *GOES-10* at 1315 UTC 13 Nov 2008 and the locations of the dropsondes. The location of each of the 10 dropsondes, labeled with the numbers, is at the cross of the longitudinal and latitudinal lines when the dropsondes reached the sea surface level.

altitude of about 100 m. Wood et al. (2011a) analyzed the 27 October 2008 case during VOCALS. They found that the along-track wind speed for a subcloud leg at 145 m MSL showed a strong cold/moist pool with low-level outflow associated with a precipitating boundary cell; that is, the convective cell separates the overcast region and the POC region.

The cold pool observed in this case was only about 200 m, which is much shallower than the 1-km-deep cold pool associated with thunderstorms (Klingle et al. 1987; Mahoney 1988) and mesoscale convective systems (Engerer et al. 2008) but similar to those observed in relatively shallow cumulus clouds and even stratocumulus clouds (e.g., Zuidema et al. 2012).

There was a sharp increase in relative humidity in the lowest 100 m in dropsonde 2, which is evidence of moistening due to evaporation of raindrops. Dropsonde 3 measured a much larger increase in horizontal wind speed than dropsonde 2, whereas an increase in relative humidity was only measured by dropsonde 2. It appears from Fig. 13 as though dropsonde 3 fell into the region of the boundary cell between open cells and the overcast region (Wood et al. 2011a), while dropsonde 2 fell into the region of open cells.

5. Discussion

Figure 15 shows a schematic diagram of the clouds and boundary layer on 13 November 2008, derived from the observations made by the BAe 146 research aircraft and the dropsondes. The aircraft flew along the 20°S latitude from 72° to 81°W off the coast of South America. The air in the MBL is more polluted near the coast, less polluted offshore, and very clean over the remote ocean. As a result, the cloud drop number concentration was highest near the coast and gradually decreased offshore and the

concentration of drops larger than 50 μm increased dramatically with distance offshore. Drizzle therefore formed in the offshore clouds, which helped to break up the Sc clouds. Evaporative cooling of the drizzle drops decoupled the MBL. Convective available potential energy built up in the decoupled MBL and shallow cumulus clouds developed under the Sc cloud.

Convective cells were observed farther offshore in a region where a POC had just started to develop. Satellite images in Fig. 1 shows the development of the POC in horizontal extent with more clear air at a later time. The interactions between cold pools, resulting from evaporative cooling of rain below cloud bases, can play an important role in the development of the convective cells and can significantly influence the distribution pattern of the clouds. The formation of open cells is related to increased drizzle, reduced concentration of the accumulated mode aerosol, and weak wind shear.

The interactions between dynamics and microphysics are often impossible to disentangle. Bretherton et al. (2010) investigated the stratocumulus clouds, precipitation, and boundary layer structure sampled along 20°S from 16 October to 15 November 2008 using airborne,

TABLE 1. Location where the sondes reached the lowest level.

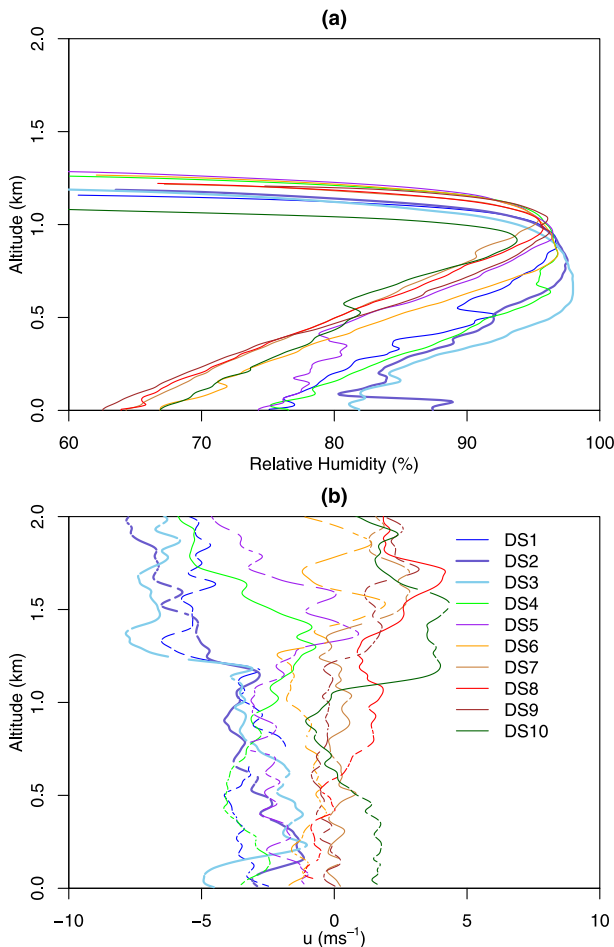| Latitude (°S)	Longitude (°W)
19.991	79.843
19.978	78.995
19.983	78.007
19.985	77.001
19.985	75.997
19.993	75.012
20.008	73.989
19.995	73.573
19.992	73.006
19.983	71.998

FIG. 14. Vertical profiles of (a) relative humidity and (b) u component of wind speed made with 10 dropsondes. Note that the thick lines are used for DS2 and DS3 to highlight the signals of the cold pools. See Fig. 13 and Table 1 for locations.

ship-based, and land-based observations during VOCALS. They suggested that other factors should be considered when interpreting correlations between cloud properties and aerosol. For example, the deepening of the MBL is associated with large-scale conditions above the MBL along 20°S. The depth of the MBL and the mesoscale variability in liquid water path play an important role in affecting cloud properties.

On 13 November 2008, the moisture and stability above the MBL did not change much along the flight track. The cloud-base and -top heights measured in profile run P9 were 760 and 1340 m, respectively. In P14, they were 845 and 1190 m, respectively. In P18, the cloud-base and -top heights were 760 and 1120 m, respectively, similar to those in P14. The cloud layers were thicker in P9 than in P14 and P18. However, the concentration of drizzle drops was much lower in in-cloud run A, prior to the profile run P9, than in runs B and C. For runs B and C, the depths of the

cloud layers were similar, but the CDNC in run C was higher than in run B as a result of decreasing aerosol concentration offshore. The concentration of drizzle drops was higher in run C than in run B. The air temperatures near the surface changed very little. At each end of the profile runs P5, P8, P14, and P18, the temperatures were 290.7, 289.8, 289.3, and 289.3 K, respectively. The SSTs were higher to the east of 75°W, which means the heat fluxes were even weaker to the west, where the concentration of drizzle drops was higher.

N50 varied significantly along 20°W in this case. Both runs A and B were carried out in solid cloud layers. In run A (between 73.478° and 74.144°W), N50 was only a few drops per liter, while the concentrations of all drops smaller than 50 μm obtained from the CDP were about 270 cm^{-3}. This means that the ratio of N50 to total drop number concentration was only 1:100 000. The concentration of drizzle drops (larger than 100 μm in diameter), N100, in run A was surprisingly not zero but was very low. In run B (between 75.963° and 76.623°W), the mean value of N50 was about 20 L^{-1}. In the open cells of run C, the ratio of N50 to total drop number concentration was about 1:100, which was about 2–3 orders of magnitude higher than in the Sc clouds. Farther to the west (between 80.5° and 81.1°W) in run D, the ratio becomes smaller in the closed cells than in the open cells. The longitudinal variations in N50 are clearly related to the variations in N100, as expected.

Wood et al. (2011a) presented a detailed study of a POC on 27–28 October 2008. They compared the well-developed POC with its surrounding overcast stratocumulus. They suggested that drizzle is not a sufficient condition for POC formation because the surrounding clouds did not turn to cellular cells and remained overcast. They proposed a POC formation hypothesis: "long-lived stratocumulus clouds with areal-mean LWP values of greater than 300 g m^{-2} cannot be sustained against coalescence losses under any conditions found during VOCALS-REx" (p. 2367). For typical drop number concentrations of about 100 cm^{-3}, a value of LWP greater than 300 g m^{-2} will produce drizzle to scavenge so many aerosol particles that other sources of aerosol are not enough to support cloud formation. The limited observations from the early stages of the development of a POC presented in this paper perhaps suggest that LWP alone is not sufficient, but the drizzle rate may also be important.

The observations made in the case discussed in this paper suggest that the microphysics dominate in the production of drizzle: the evidence suggests that the principal factor was the concentration of cloud drops. Presumably this is because a sustainable balance between cloud depth and cloud drop concentration was not achieved in these Sc clouds.
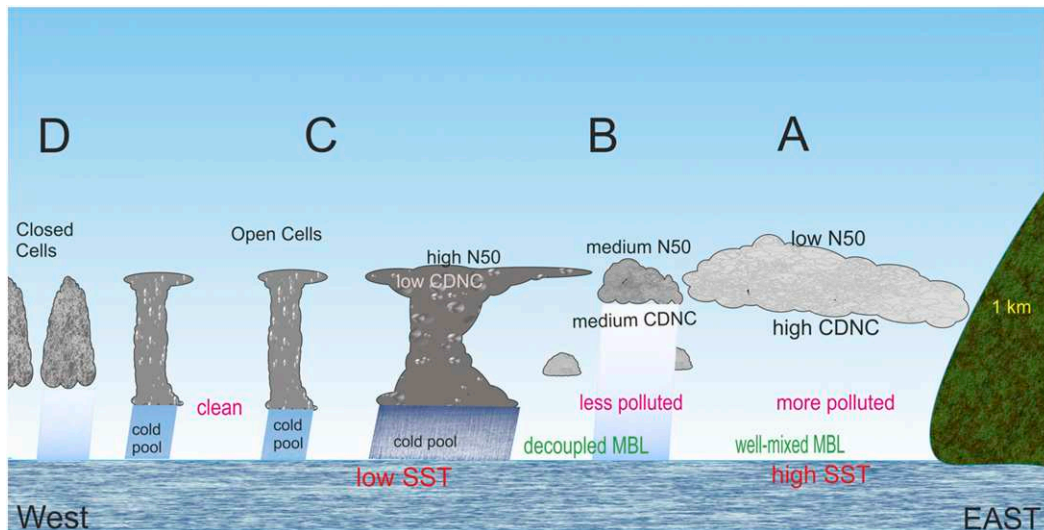
FIG. 15. Schematic figure of regime shift in an aerosol–cloud–precipitation system along 20°S latitude for the case observed on 13 Nov 2008. See text for details.

6. Summary

Observations were made with the BAe 146 aircraft on 13 November 2008 along 20°S latitude from the coast of Chile to slightly west of 81°W, in order to determine the variations in clouds, the MBL, and aerosol along the transect. Mesoscale cellular clouds developed and moved across 20°S from southeast to northwest. The early stages of development of a POC were also observed. There were significant longitudinal variations in aerosol particles and cloud properties. The largest concentration of aerosol was about $700 \, cm^{-3}$, observed between 74° and 75°W. The concentration was slightly lower than this maximum to the east and much lower to the west. The variation in cloud drop number concentration was correlated with the variation in aerosol concentration, as expected. The concentration of cloud drops was about $100–300 \, cm^{-3}$ to the east of the POC and less than $100 \, cm^{-3}$ in the POC region. Drizzle drops were observed in the stratocumulus clouds, with small concentrations at about 76°W and larger concentrations farther west, with the greatest concentration in the POC region. The ratios of the concentration of drops larger than $50 \, \mu m$ to the total drop concentration measured with the CDP were significantly different in the POC and in the Sc clouds, as expected. In the POC region, the ratios were between 1:10 and 1:100, but much lower in the Sc clouds. The lack of drizzle in the Sc meant the clouds could persist for a long time. The warm rain process is more efficient in the POC region. The cooling through the evaporation of drizzle drops below cloud base caused downdrafts that stabilize the boundary layer. The cold pools can trigger new cloud formation at the edge of the cloudy walls between the open, clear air. The interaction between aerosol, cloud, and drizzle is largely controlled by microphysics. A schematic model is proposed to explain the observed transition from overcast to open cells.

REFERENCES

Allen, G., and Coauthors, 2011: South east Pacific atmospheric composition and variability sampled along 20°S during VOCALS-REx. *Atmos. Chem. Phys.,* **11,** 5237–5262, doi:10.5194/acp-11-5237-2011.

Andreae, M. O., W. Elbert, Y. Cai, T. W. Andreae, and J. Gras, 1999: Non-sea-salt sulfate, methanesulfonate, and nitrate aerosol concentrations and size distributions at Cape Grim, Tasmania. *J. Geophys. Res.,* **104,** 21 695–21 706, doi:10.1029/1999JD900283.

Artaxo, P., P. Oyola, and R. Martinez, 1999: Aerosol composition and source apportionment in Santiago de Chile. *Nucl. Instrum. Methods Phys. Res.,* **150B,** 409–416, doi:10.1016/S0168-583X(98)01078-7.

Ayers, G. P., J. P. Ivey, and R. W. Gillett, 1991: Coherence between seasonal cycles of dimethyl sulfide, methanesulphonate and sulphate in marine air. *Nature,* **349,** 404–406, doi:10.1038/349404a0.

Bennartz, R., 2007: Global assessment of marine boundary layer cloud droplet number concentration from satellite. *J. Geophys. Res.,* **112,** D02201, doi:10.1029/2006JD007547.

Bennetts, D. A., E. McCallum, S. Nicholl, and J. R. Grant, 1986: Stratocumulus: An introductory account. *Meteor. Mag.,* **115,** 65–76.

Betts, A. K., 1973: Non-precipitating convection and its parameterization. *Quart. J. Roy. Meteor. Soc.,* **99,** 178–196, doi:10.1002/qj.49709941915.

Blyth, A. M., J. H. Lowenstein, Y. Huang, Z. Cui, S. Davies, and K. S. Carslaw, 2013: The production of warm rain in shallow maritime cumulus clouds. *Quart. J. Roy. Meteor. Soc.,* **139,** 20–31, doi:10.1002/qj.1972.

Bretherton, C. S., and M. C. Wyant, 1997: Moisture transport, lower-tropospheric stability, and decoupling of cloud-topped boundary layers. *J. Atmos. Sci.,* **54,** 148–167, doi:10.1175/1520-0469(1997)054<0148:MTLTSA>2.0.CO;2.

——, and Coauthors, 2004: The EPIC 2001 stratocumulus study. *Bull. Amer. Meteor. Soc.,* **85,** 967–977, doi:10.1175/BAMS-85-7-967.

——, R. Wood, R. C. George, D. Leon, G. Allen, and X. Zheng, 2010: Southeast Pacific stratocumulus clouds, precipitation and boundary layer structure sampled along 20°S during VOCALS-REx. *Atmos. Chem. Phys.,* **10,** 10 639–10 654, doi:10.5194/acp-10-10639-2010.

Brost, R. A., J. C. Wyngaard, and D. H. Lenschow, 1982: Marine stratocumulus layers. Part II: Turbulence budgets. *J. Atmos. Sci.,* **39,** 818–836, doi:10.1175/1520-0469(1982)039<0818:MSLPIT>2.0.CO;2.

Carn, S. A., A. J. Krueger, N. A. Krotkov, K. Yang, and P. F. Levelt, 2007: Sulfur dioxide emissions from Peruvian copper smelters detected by the Ozone Monitoring Instrument. *Geophys. Res. Lett.,* **34,** L09801, doi:10.1029/2006GL029020.

Chand, D., D. A. Hegg, R. Wood, G. E. Shaw, D. Wallace, and D. S. Covert, 2010: Source attribution of climatically important aerosol properties measured at Paposo (Chile) during VOCALS. *Atmos. Chem. Phys.,* **10,** 10 789–10 801, doi:10.5194/acp-10-10789-2010.

Comstock, K. K., C. S. Bretherton, and S. E. Yuter, 2005: Mesoscale variability and drizzle in southeast Pacific stratocumulus. *J. Atmos. Sci.,* **62,** 3792–3807, doi:10.1175/JAS3567.1.

——, S. E. Yuter, R. Wood, and C. S. Bretherton, 2007: The three-dimensional structure and kinematics of drizzling stratocumulus. *Mon. Wea. Rev.,* **135,** 3767–3784, doi:10.1175/2007MWR1944.1.

Crawford, I., and Coauthors, 2012: Ice formation and development in aged, wintertime cumulus over the UK: Observations and modelling. *Atmos. Chem. Phys.,* **12,** 4963–4985, doi:10.5194/acp-12-4963-2012.

Crosier, J., and Coauthors, 2011: Observations of ice multiplication in a weakly convective cell embedded in supercooled mid-level stratus. *Atmos. Chem. Phys.,* **11,** 257–273, doi:10.5194/acp-11-257-2011.

——, and Coauthors, 2014: Microphysical properties of cold frontal rainbands. *Quart. J. Roy. Meteor. Soc.,* **140,** 1257–1268, doi:10.1002/qj.2206.

Cui, Z., A. M. Blyth, K. N. Bower, J. Crosier, and T. Choularton, 2012: Aircraft measurements of wave clouds. *Atmos. Chem. Phys.,* **12,** 9881–9892, doi:10.5194/acp-12-9881-2012.

Drewnick, F., and Coauthors, 2005: A new time-of-flight aerosol mass spectrometer (TOF-AMS)—Instrument description and first field deployment. *Aerosol Sci. Technol.,* **39,** 637–658, doi:10.1080/02786820500182040.

Engerer, N. A., D. J. Stensrud, and M. C. Coniglio, 2008: Surface characteristics of observed cold pools. *Mon. Wea. Rev.,* **136,** 4839–4849, doi:10.1175/2008MWR2528.1.

Feind, R. E., A. G. Detwiler, and P. L. Smith, 2000: Cloud liquid water measurements on the armored T-28: Intercomparison between Johnson–Williams cloud water meter and CSIRO (King) liquid water probe. *J. Atmos. Oceanic Technol.,* **17,** 1630–1638, doi:10.1175/1520-0426(2000)017<1630:CLWMOT>2.0.CO;2.

Gerber, H., G. Frick, S. P. Malinowski, J.-L. Brenguier, and F. Burnet, 2005: Holes and entrainment in stratocumulus. *J. Atmos. Sci.,* **62,** 443–459, doi:10.1175/JAS-3399.1.

Jayne, J. T., D. C. Leard, X. Zhang, P. Davidovits, K. A. Smith, C. E. Kolb, and D. R. Worsnop, 2000: Development of an aerosol mass spectrometer for size and composition analysis of submicron particles. *Aerosol Sci. Technol.,* **33,** 49–70, doi:10.1080/027868200410840.

Jensen, J. B., S. Lee, P. B. Krummel, J. Katzfey, and D. Gogoasa, 2000: Precipitation in marine cumulus and stratocumulus. Part I: Thermodynamic and dynamic observations of closed cell circulations and cumulus bands. *Atmos. Res.,* **54,** 117–155, doi:10.1016/S0169-8095(00)00040-5.

Jones, C. R., C. S. Bretherton, and D. Leon, 2011: Coupled vs. decoupled boundary layers in VOCALS-REx. *Atmos. Chem. Phys.,* **11,** 7143–7153, doi:10.5194/acp-11-7143-2011.

Kazil, J., H. Wang, G. Feingold, A. D. Clarke, J. R. Snider, and A. R. Bandy, 2011: Modeling chemical and aerosol processes in the transition from closed to open cells during VOCALS-REx. *Atmos. Chem. Phys.,* **11,** 7491–7514, doi:10.5194/acp-11-7491-2011.

Klein, S. A., D. L. Hartman, and J. R. Norris, 1995: On the relationships among low-cloud structure, sea surface temperature, and atmospheric circulation in the summertime northeast Pacific. *J. Climate,* **8,** 1140–1155, doi:10.1175/1520-0442(1995)008<1140:OTRALC>2.0.CO;2.

Klingle, D. L., D. R. Smith, and M. M. Wolfson, 1987: Gust front characteristics as detected by Doppler radar. *Mon. Wea. Rev.,* **115,** 905–918, doi:10.1175/1520-0493(1987)115<0905:GFCADB>2.0.CO;2.

Korolev, A. V., J. W. Strapp, G. A. Isaac, and A. N. Nevzorov, 1998: The Nevzorov airborne hot-wire LWC–TWC probe: Principle of operation and performance characteristics. *J. Atmos. Oceanic Technol.,* **15,** 1495–1510, doi:10.1175/1520-0426(1998)015<1495:TNAHWL>2.0.CO;2.

Lance, S., C. A. Brock, D. Rogers, and J. A. Gordon, 2010: Water droplet calibration of the cloud droplet probe (CDP) and in-flight performance in liquid, ice and mixed-phase clouds during ARCPAC. *Atmos. Meas. Tech.,* **3,** 1683–1706, doi:10.5194/amt-3-1683-2010.

Lawson, R. P., D. O'Connor, P. Zmarzly, K. Weaver, B. Baker, Q. Mo, and H. Jonsson, 2006: The 2D-S (stereo) probe: Design and preliminary tests of a new airborne, high-speed, high-resolution particle imaging probe. *J. Atmos. Oceanic Technol.,* **23,** 1462–1477, doi:10.1175/JTECH1927.1.

Mahoney, W. P., III, 1988: Gust front characteristics and the kinematics associated with interacting thunderstorm outflows. *Mon. Wea. Rev.,* **116,** 1474–1492, doi:10.1175/1520-0493(1988)116<1474:GFCATK>2.0.CO;2.

Mari, C., and Coauthors, 1998: Physico-chemical modeling of the First Aerosol Characterization Experiment (ACE 1) Lagrangian B: 2. DMS emission, transport and oxidation at the mesoscale. *J. Geophys. Res.,* **103,** 16 457–16 473, doi:10.1029/98JD01068.

Nicholls, S., 1984: The dynamics of stratocumulus aircraft observations and comparisons with a mixed layer model. *Quart. J. Roy. Meteor. Soc.,* **110,** 783–820, doi:10.1002/qj.49711046603.

O'Dowd, C. D., and G. de Leeuw, 2007: Marine aerosol production: A review of the current knowledge. *Philos. Trans. Roy. Soc. London,* **A365,** 1753–1774, doi:10.1098/rsta.2007.2043.

——, M. H. Smith, I. E. Consterdine, and J. A. Lowe, 1997: Marine aerosol, sea-salt, and the marine sulphur cycle: A short review. *Atmos. Environ.,* **31,** 73–80, doi:10.1016/S1352-2310(96)00106-9.

Painemal, D., R. Garreaud, J. Rutllant, and P. Zuidema, 2010: Southeast Pacific stratocumulus: High-frequency variability and mesoscale structures over San Felix Island. *J. Appl. Meteor. Climatol.,* **49,** 463–477, doi:10.1175/2009JAMC2230.1.

Pawlowska, H., and J.-L. Brenguier, 2003: An observational study of drizzle formation in stratocumulus clouds for general circulation model (GCM) parameterizations. *J. Geophys. Res.,* **108,** 8630, doi:10.1029/2002JD002679.

Rahn, D. A., and R. Garreaud, 2010a: Marine boundary layer over the subtropical southeast Pacific during VOCALS-REx—Part 1: Mean structure and diurnal cycle. *Atmos. Chem. Phys.,* **10,** 4491–4506, doi:10.5194/acp-10-4491-2010.

——, and ——, 2010b: Marine boundary layer over the subtropical southeast Pacific during VOCALS-REx—Part 2: Synoptic variability. *Atmos. Chem. Phys.,* **10,** 4507–4519, doi:10.5194/acp-10-4507-2010.

Savic-Jovcic, V., and B. Stevens, 2008: The structure and mesoscale organization of precipitating stratocumulus. *J. Atmos. Sci.,* **65,** 1587–1605, doi:10.1175/2007JAS2456.1.

Shank, L. M., and Coauthors, 2012: Organic matter and non-refractory aerosol over the remote southeast Pacific: Oceanic and combustion sources. *Atmos. Chem. Phys.,* **12,** 557–576, doi:10.5194/acp-12-557-2012.

Sharon, T. M., B. A. Albrecht, H. H. Jonsson, P. Minnis, M. M. Khaiyer, T. M. van Reken, J. Seinfeld, and R. Flagan, 2006: Aerosol and cloud microphysical characteristics of rifts and gradients in maritime stratocumulus clouds. *J. Atmos. Sci.,* **63,** 983–997, doi:10.1175/JAS3667.1.

Sievering, H., J. Boatman, E. Gorman, Y. Kim, L. Anderson, G. Ennis, M. Luria, and S. Pandis, 1992: Removal of sulphur from the marine boundary layer by ozone oxidation in sea-salt aerosols. *Nature,* **360,** 571–573, doi:10.1038/360571a0.

Stevens, B., G. Vali, K. Comstock, R. Wood, M. C. Van Zanten, P. H. Austin, C. S. Bretherton, and D. H. Lenschow, 2005: Pockets of open cells and drizzle in marine stratocumulus. *Bull. Amer. Meteor. Soc.,* **86,** 51–57, doi:10.1175/BAMS-86-1-51.

Strapp, J. W., and R. S. Schemenauer, 1982: Calibrations of Johnson–Williams liquid water content meters in a high-speed icing tunnel. *J. Appl. Meteor.,* **21,** 98–108, doi:10.1175/1520-0450(1982)021<0098:COJWLW>2.0.CO;2.

Tomlinson, J. M., R. Li, and D. R. Collins, 2007: Physical and chemical properties of the aerosol within the southeastern Pacific marine boundary layer. *J. Geophys. Res.,* **112,** D12211, doi:10.1029/2006JD007771.

Toniazzo, T., S. J. Abel, R. Wood, C. R. Mechoso, G. Allen, and L. C. Shaffrey, 2011: Large-scale and synoptic meteorology in the south-east Pacific during the observations campaign VOCALS-REx in austral spring 2008. *Atmos. Chem. Phys.,* **11,** 4977–5009, doi:10.5194/acp-11-4977-2011.

Wood, R., 2012: Stratocumulus clouds. *Mon. Wea. Rev.,* **140,** 2373–2423, doi:10.1175/MWR-D-11-00121.1.

——, and C. S. Bretherton, 2004: Boundary layer depth, entrainment, and decoupling in the cloud-capped subtropical and tropical marine boundary layer. *J. Climate,* **17,** 3576–3588, doi:10.1175/1520-0442(2004)017<3576:BLDEAD>2.0.CO;2.

——, ——, D. Leon, A. D. Clarke, P. Zuidema, G. Allen, and H. Coe, 2011a: An aircraft case study of the spatial transition from closed to open mesoscale cellular convection over the southeast Pacific. *Atmos. Chem. Phys.,* **11,** 2341–2370, doi:10.5194/acp-11-2341-2011.

——, and Coauthors, 2011b: The VAMOS Ocean–Cloud–Atmosphere–Land Study Regional Experiment (VOCALS-REx): Goals, platforms, and field operations. *Atmos. Chem. Phys.,* **11,** 627–654, doi:10.5194/acp-11-627-2011.

——, D. Leon, M. Lebsock, J. Snider, and A. D. Clarke, 2012: Precipitation driving of droplet concentration variability in marine low clouds. *J. Geophys. Res.,* **117,** D19210, doi:10.1029/2012JD018305.

Yum, S. S., and J. G. Hudson, 2004: Wintertime/summertime contrasts of cloud condensation nuclei and cloud microphysics over the Southern Ocean. *J. Geophys. Res.,* **109,** D06204, doi:10.1029/2003JD003864.

Zuidema, P., D. Painemal, S. de Szoeke, and C. Fairall, 2009: Stratocumulus cloud-top height estimates and their climatic implications. *J. Climate,* **22,** 4652–4666, doi:10.1175/2009JCLI2708.1.

——, and Coauthors, 2012: On trade wind cumulus cold pools. *J. Atmos. Sci.,* **69,** 258–280, doi:10.1175/JAS-D-11-0143.1.